Murine HSCs contribute actively to native hematopoiesis but with reduced differentiation capacity upon aging

Petter Säwen[1], Mohamed Eldeeb[1], Eva Erlandsson[1], Trine A Kristiansen[1], Cecilia Laterza[2,3], Zaal Kokaia[2,3], Göran Karlsson[1,2,3], Joan Yuan[1,2,3], Shamit Soneji[1,2,3], Pankaj K Mandal[4,5], Derrick J Rossi[4,5], David Bryder[1,2,3,6]*

[1]Division of Molecular Hematology, Department of Laboratory Medicine, Medical Faculty, Lund University, Lund, Sweden; [2]StemTherapy, Lund University, Lund, Sweden; [3]Lund Stem Cell Center, Lund University, Lund, Sweden; [4]Department of Stem Cell and Regenerative Biology, Harvard University, Cambridge, United States; [5]Program in Cellular and Molecular Medicine, Division of Hematology/Oncology, Boston Children's Hospital, Massachusetts, United States; [6]Sahlgrenska Cancer Center, Gothenburg University, Gothenburg, Sweden

Abstract A hallmark of adult hematopoiesis is the continuous replacement of blood cells with limited lifespans. While active hematopoietic stem cell (HSC) contribution to multilineage hematopoiesis is the foundation of clinical HSC transplantation, recent reports have questioned the physiological contribution of HSCs to normal/steady-state adult hematopoiesis. Here, we use inducible lineage tracing from genetically marked adult HSCs and reveal robust HSC-derived multilineage hematopoiesis. This commences via defined progenitor cells, but varies substantially in between different hematopoietic lineages. By contrast, adult HSC contribution to hematopoietic cells with proposed fetal origins is neglible. Finally, we establish that the HSC contribution to multilineage hematopoiesis declines with increasing age. Therefore, while HSCs are active contributors to native adult hematopoiesis, it appears that the numerical increase of HSCs is a physiologically relevant compensatory mechanism to account for their reduced differentiation capacity with age.
DOI: https://doi.org/10.7554/eLife.41258.001

*For correspondence: david.bryder@med.lu.se

Introduction

HSC-derived hematopoiesis has usually been studied in the setting of transplantation (*Benz et al., 2012*; *Biasco et al., 2016*; *Dykstra et al., 2007*; *Lu et al., 2011*; *Rundberg Nilsson et al., 2015*; *Wu et al., 2014*), an experimental paradigm that has been the foundation of hematopoietic research for decades (*Siminovitch et al., 1963*; *Till and McCulloch, 1961*) and which has established hallmark properties of HSCs such as multi-potency and self-renewal. However, while the transplantation assay has provided key insights, not the least with relevance for the clinical use in bone marrow (BM) transplantation, it might not accurately reflect the contribution of HSCs to ongoing and unperturbed steady state hematopoiesis. This is because transplantation is conducted under highly non-physiological conditions wherein HSCs are forced to proliferate to rebuild an entire hematopoietic hierarchy in a myeloablated bone marrow micro-environment. Therefore, there is a need to approach HSC biology also in more unperturbed settings.

While the overall structure of hematopoiesis is rather well established (*Bryder et al., 2006*), the degree by which HSCs contribute to adult hematopoiesis in the steady state is more unclear. This includes whether the proposed differentiation routes for the hematopoietic lineages are obligatory,

eLife digest As far as we know, all adult blood cells derive from blood stem cells that are located in the bone marrow. These stem cells can produce red blood cells, white blood cells and platelets – the cells fragments that form blood clots to stop bleeding. They can also regenerate, producing more stem cells to support future blood cell production. But, our understanding of the system may be incomplete.

The easiest way to study blood cell production is to watch what happens after a bone marrow transplant. Before a transplant, powerful chemotherapy kills the existing stem cells. This forces the transplanted stem cells to restore the whole system from scratch, allowing scientists to study blood cell production in fine detail. But completely replacing the bone marrow puts major stress on the body, and this may alter the way that the stem cells behave. To understand how adult stem cells keep the blood ticking over on a day-to-day basis, experiments also need to look at healthy animals.

Säwén et al. now describe a method to follow bone marrow stem cells as they produce blood cells in adult mice. The technique, known as lineage tracing, leaves an indelible mark, a red glow, on the stem cells. The cells pass this mark on every time they divide, leaving a lasting trace in every blood cell that they produce. Tracking the red-glowing cells over time reveals which types of blood cells the stem cells make as well as provides estimates on the timing and extent of these processes.

It has previously been suggested that a few types of specialist blood cells, like brain-specific immune cells, originate from cells other than adult blood stem cells. As expected, the adult stem cells did not produce such cells. But, just as seen in transplant experiments, the stem cells were able to produce all the other major blood cell types. They made platelets at the fastest rate, followed by certain types of white blood cells and red blood cells. As the mice got older, the stem cells started to slow down, producing fewer blood cells each. To compensate, the number of stem cells increased, helping to keep blood cell numbers up.

This alternative approach to studying blood stem cells shows how the system behaves in a more natural environment. Away from the stresses of transplant, the technique revealed that blood stem cells are not immune to aging. In the future, understanding more about the system in its natural state could lead to ways to boost blood stem cells as we get older.

DOI: https://doi.org/10.7554/eLife.41258.002

or whether alternative/complementary pathways exist. Furthermore, cells of the different hematopoietic lineages have not only distinct homeostatic functions and maintenance mechanisms (*Bando and Colonna, 2016*; *Dzierzak and Philipsen, 2013*; *Rodvien and Mielke, 1976*) but also display dramatically different lifespans (*Galli et al., 2011*; *Harker et al., 2000*; *Van Putten, 1958*; *Westera et al., 2013*). As a consequence, the rates by which separate adult-derived blood cell lineages must be replenished differ substantially. At the extreme end, certain hematopoietic cell types generated during the fetal period appear devoid of replenishment from adult progenitors, and rather rely on homeostatic proliferation for their maintenance (*Ginhoux and Guilliams, 2016*; *Kantor et al., 1995*).

Recent developments of transgenic mouse models that allow for identification (*Acar et al., 2015*; *Chen et al., 2016*; *Gazit et al., 2014*) and evaluation of HSCs biology have facilitated studies of native in vivo hematopoiesis (*Busch et al., 2015*; *Sawai et al., 2016*; *Sun et al., 2014*; *Wilson et al., 2008*). Using one such model, we recently revealed that most adult HSCs are highly quiescent, which is strikingly different in the transplantation scenario (*Säwén et al., 2016*). Other models have been used for lineage tracing from HSCs (*Busch et al., 2015*; *Sawai et al., 2016*; *Sun et al., 2014*). In one of these, lineage tracing was conducted via random genetic integration of an inducible transposable genetic element, leading to the proposition that native hematopoiesis involves a large number of actively contributing progenitor cell clones, which are only rarely shared among hematopoietic lineages (*Sun et al., 2014*). More common approaches for lineage tracing involve the use of cell type specific recombinases, that function to irreversibly mark a cell of interest and with time its descendants. While elegant and extensively used among developmental biologists, such approaches have only sparsely been applied to adult HSCs, and with seemingly contradictory results. Using a Tie2-driven model, Busch et al. concluded a substantial hematopoietic contribution/maintenance from progenitors rather than HSCs (*Busch et al., 2015*), which at least to some extent would appear

compatible with the results from *Sun et al. (2014)*. By contrast, Sawai et al. utilized a Pdzk1ip1-based CreERT2 system and suggested robust HSC labeling and hematopoiesis from adult HSCs (*Sawai et al., 2016*).

To try to assess these potential ambiguities, we here investigated the degree to which HSCs contribute to steady state adult hematopoiesis by using an inducible Fgd5-based HSC lineage tracing model (*Gazit et al., 2014*). We observed dramatic differences with regards to HSC contribution to adaptive immunity (slow) and the myeloerythroid lineages (fast), with HSCs contributing to the platelet lineage with the most rapid kinetics. The regeneration of terminal cell fates was closely mirrored at the level of each intermediate myeloerythroid precursor. These findings are consistent with adult HSCs as highly active contributors to multilineage hematopoiesis not only following transplantation, but also during the steady state. However, when approached in the situation of chronological aging, we noted diminished mature blood cell output from aged HSCs that could be traced to the first differentiation events from HSCs. These results suggest that the previously proposed fetal to adult switch (*Bowie et al., 2007*), in which HSCs alter their properties from more excessive proliferation/differatiation to a more dormant state in the adult, extends gradually throughout adulthood. As a consequence, the well-known numerical increase of HSCs with age (*Morrison et al., 1996*; *Rossi et al., 2005*; *Sudo et al., 2000*) appears to represent a physiologically relevant mechanism to account for reduced HSC differentiation with age.

Results

Fgd5-CreERT2-based lineage tracing allows for assessment of HSC contributions to unperturbed hematopoiesis

Using a transcriptome based screen of more than 40 different hematopoietic cell types, Fgd5 (FYVE, RhoGEF and PH domain containing 5) was identified as a HSC-expressed gene that is rapidly down-regulated upon differentiation. That Fgd5 expression marks all HSCs was confirmed through functional studies using an Fgd5 knock-in reporter strain (*Gazit et al., 2014*). To further detail the HSC specificity of Fgd5, we first acquired transcriptome data from 11,581 individual lineage-marker negative, c-kit positive and CD45 positive bone marrow cells (Lin^-kit^+). The Lin^-kit^+ population contains a range of different immature hematopoietic progenitor cells (*Pronk et al., 2007*). Therefore, Lin^-kit^+ cells provided a benchmark to which other more defined/specific hematopoietic progenitor subsets could be compared. Next, we took advantage of an Fgd5 reporter strain in which a ZsGreen-2A-CreERT2 allele was knocked into the endogenous *Fgd5* locus (hereafter *Fgd5$^{CreERT2/+}$* mice) (*Figure 1B*) (*Gazit et al., 2014*). We sorted either $Lin^-kit^+Fgd5^+$ cells (*Figure 1A* middle; 793 cells, $Fgd5^+$), or $Fgd5^+$ cells with a stringent $Lin^-kit^+Sca-1^+CD48^-CD150^+$ HSC phenotype (*Figure 1A* right, 519 cells, $HSC-Fgd5^+$). All $Fgd5^+$ and $HSC-Fgd5^+$ data were aggregated with the Lin^-kit^+ transcriptome data, which was followed by identification of the most significant gene vectors using principal component analysis (PCA). Data was then visualized using t-distributed stochastic neighbor embedding (tSNE) dimensionality reduction (*Figure 1A*). Lin^-kit^+ cells were extensively scattered across the two dimensions (*Figure 1A*, left), in agreement with the heterogeneity of these cells. By contrast, $Fgd5^+$ cells, regardless if sorted based on additional HSC markers, formed a distinct and highly overlapping cluster (*Figure 1A*, middle and right). This cluster localized to a region with very few cells when evaluating Lin^-kit^+ cells (*Figure 1A*, left, dotted area), emphasizing the HSC-specificity of the Fgd5 reporter and the low HSC frequency within the larger Lin^-kit^+ fraction.

We next generated a lineage tracing model by crossing *Fgd5$^{CreERT2/+}$* mice to *Rosa26-Lox-Stop-Lox-Tomato* mice (hereafter *Rosa26$^{lsl-Tomato/+}$*) (*Figure 1B*). In this model, HSCs can be identified based on ZsGreen expression, while Tamoxifen administration leads to irreversible and heritable Tomato labeling of HSCs and, over time, their offspring (*Figure 1C*). To confirm the model, we evaluated Tomato label in HSC and BM progenitor cells 48 hr after a single injection (1x) of Tamoxifen. This revealed labeling of a fraction of candidate HSCs, with virtually no labeling in other $c-kit^+$ progenitor fractions (*Figure 1D* and *Figure 1—figure supplement 1*). This established HSC specific labeling and a relatively low differentiation rate of HSCs in steady state (*Säwén et al., 2016*; *Wilson et al., 2008*). To illustrate our ability to detect Tomato label in peripheral blood (PB) cells, we assessed Tomato expression in defined cell types from mice that had received Tamoxifen 8–48 weeks previously (*Figure 1D*, lower right). Complementary to immunophenotypic identification of
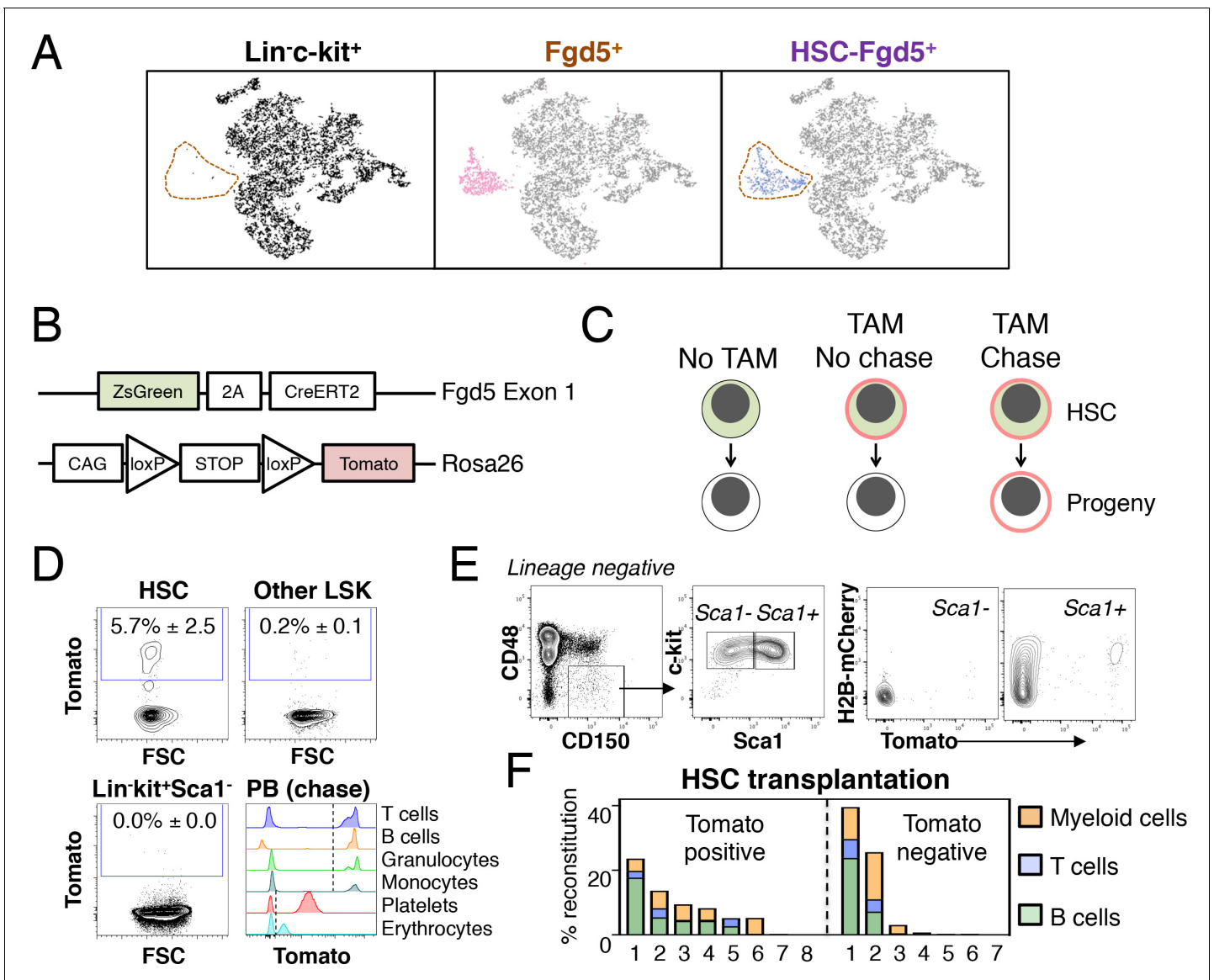
Figure 1. Fgd5-CreERT2 specifically labels HSCs and Fgd5-mediated label progresses throughout the hematopoietic system. (A) Lineage negative c-kit$^+$ cells (Lin$^-$c-kit$^+$, left), lineage negative c-kit$^+$ Fgd5$^+$ cells (Fgd5$^+$, middle) and lineage negative Fgd5$^+$c-kit$^+$Sca-1$^+$CD150$^+$CD48$^-$ cells (HSC-Fgd5$^+$, right) were isolated and subjected to single cell RNA-sequencing. The data was aggregated and visualized in a two-dimensional scatter plot after PCA and tSNE dimensionality reduction. Fgd5$^+$ cells are highlighted in pink (middle), Lin$^-$c-kit$^+$ cells are highlighted in black (left plot) and HSC-Fgd5$^+$ cells are highlighted in blue (right plot). The area that Fgd5$^+$ cells occupy in relation to the transcriptomes of Lin$^-$c-kit$^+$ cells and HSC-Fgd5$^+$ cells is marked by a dotted line (left and right plots). (B) Schematic representation of the $Fgd5^{CreERT2/+}$; $Rosa26^{lsl-Tomato/+}$ model. ZsGreen and CreERT2 are expressed from the Fgd5 locus and expression of a Tomato allele is driven by a CAG promoter from the Rosa26 locus and is preceded by a LoxP flanked STOP cassette. (C) Model description; HSCs selectively and continuously express ZsGreen in an Fgd5-dependent manner. Upon Tamoxifen (TAM) administration, HSCs express Tomato and expression of Tomato label is inherited by all progeny of Tomato-expressing HSCs. (D) Representative FACS plots showing Tomato label in BM HSPCs from $Fgd5^{CreERT2/+}$; $Rosa26^{lsl-Tomato/+}$ mice that were injected with Tamoxifen 48 hr prior to analysis. (D, lower right) Representative histograms depicting Tomato label in PB cells at various time points after the start of Tamoxifen administration from mice in *Figure 3B* (T cells 48 weeks, B cells 25 weeks, granulocytes and monocytes 8 weeks, platelets and erythrocytes 13 weeks). Numbers in FACS plots depict the mean % of Tomato labeled cells ± SD (n = 5) and dashed lines in histograms indicates the boundary for Tomato positivity. (E) FACS plots showing H2B-mCherry label retention and Tomato labeling in Lineage$^-$c-kit$^+$CD150$^+$CD48$^-$ and Sca1$^+$ or Sca1$^-$ cells from a representative mouse that had diluted H2B-mCherry label for 5 weeks and were injected with Tamoxifen 5 days prior to analysis (n = 3; 14–19 weeks old at analysis). (F) The fraction of donor-derived cells among different blood cell lineages was assessed in individual mice 16 weeks post-transplantation in recipients of 5 Tomato$^+$ (n = 8) or 5 Tomato$^-$ (n = 7) HSCs. Abbreviations: 2A, 2A self-cleaving peptide; CAG, CAG promoter; loxP, LoxP site.

The following figure supplement is available for figure 1:

Figure 1 continued on next page

initially labeled BM cells as HSCs (*Figure 1D* and data not shown), we evaluated the proliferation history of Tomato labeled HSPCs 5 days after a pulse of Tomato labeling by evaluation of transgenic H2B-mCherry label retention (*Figure 1E*) (*Säwén et al., 2016*). Among HSCs, this revealed a strong correlation between a restricted proliferative history and Tomato labeling. Of note, a single dose of Tamoxifen was insufficient to label all candidate Fgd5-expressing HSCs (*Figure 1E* and data not shown).

Finally, to corroborate that Tomato labeled phenotypic HSCs are bona fide HSCs, we injected mice with Tamoxifen and isolated candidate Tomato positive and negative HSCs 48 hr later. Sorted cells were transplanted at limiting dilution (5 cells/mouse). This revealed long-term multilineage reconstitution in 5/8 recipients transplanted with Tomato$^+$ HSCs (*Figure 1F*).

Fgd5-lineage tracing reveals that HSCs generate different types of hematopoietic progeny with distinct kinetics

Encouraged by the highly specific HSC label observed after Tamoxifen administration to *Fgd5$^{CreERT2/+}$*; *Rosa26$^{lsl-Tomato/+}$* mice (*Figure 1*), we next set out to perform label tracing studies of hematopoietic generation from HSCs. For this, we labeled cohorts of *Fgd5$^{CreERT2/+}$*; *Rosa26$^{lsl-Tomato/+}$* mice with one injection of Tamoxifen and chased groups of mice for different periods of time up to 83 weeks after labeling. At end point analyses, the fraction of Tomato$^+$ cells was determined in various hematopoietic compartments to assess the HSC contribution to progenitor pools and mature blood cell subsets (*Figure 1—figure supplement 1*). The frequencies of Tomato$^+$ cells for each investigated subset were next related to the fraction of Tomato labeled HSCs (*Figure 2A*, mean 13% ± 9%) in individual mice (*Figure 2B*, and *Figure 2—figure supplement 1*). The fraction of labeled HSCs was generally higher in mice analyzed beyond 4 days of chase compared to mice analyzed after shorter chase periods. However, no further increase in HSC labeling was noted after longer periods of chase (*Figure 2A*).

First, we investigated Tomato label progression into the immature lineage negative, Sca-1 positive and c-kit positive (LSK) compartment, fractionated further using the Slam markers CD48 and CD150 (*Kiel et al., 2005*) (*Figure 2B* and *Figure 1—figure supplement 1*). We used this approach to identify HSCs (LSKCD150$^+$CD48$^-$) and different multipotent progenitor fractions (MPPs: LSKCD150$^-$CD48$^-$, MPP^2: LSKCD150$^+$CD48$^+$, MPP$^{3/4}$: LSKCD150$^-$CD48$^+$).

LSKCD150$^-$CD48$^-$ MPPs are immature multipotent progenitors distinguished from HSCs by their limited self-renewal potential (*Kiel et al., 2005*; *Kiel et al., 2008*; *Ugale et al., 2014*). Of the evaluated progenitor subsets in our work, this subset was generated from HSCs with the fastest kinetics, with near equilibrium to HSC label reached already by 4 weeks (*Figure 2B*).

MPP^2 cells represent a rare subset of cells with more undefined lineage/developmental affiliations. This prompted us to first elucidate their developmental potential. First, we aimed to place these cells within a transcriptional framework established by other, more established, hematopoietic progenitors. For this, we obtained gene expression data from a panel of defined stem and progenitor cells and MPP^2 cells using a multiplexed qRT-PCR approach for 48 genes, selected to include cell surface markers, cell cycle regulators and transcription factors associated with hematopoiesis (*Supplementary file 2*). Visualization of this data using PCA revealed that MPP^2 cells clustered closely to Meg/E progenitors (*Figure 2C*). Consistent with a close association to the Meg/E lineages, short-term (6 days) culture experiments revealed a more robust generation of both megakaryocyte and erythroid containing colonies from MPP^{2}s compared to other LSK subsets (*Figure 2—figure supplement 2*). When investigating Tomato label progression, MPP^2 cells reached label equilibrium with HSCs after 32 weeks in 1x injected mice (*Figure 2B*).

MPP$^{3/4}$ cells lack, for the most part, Meg/E lineage potential (*Adolfsson et al., 2005*; *Arinobu et al., 2007*; *Pietras et al., 2015*; *Pronk et al., 2007*). MPP$^{3/4}$ cells acquired Tomato label with much slower kinetics compared to other LSK fractions (*Figure 2B*).
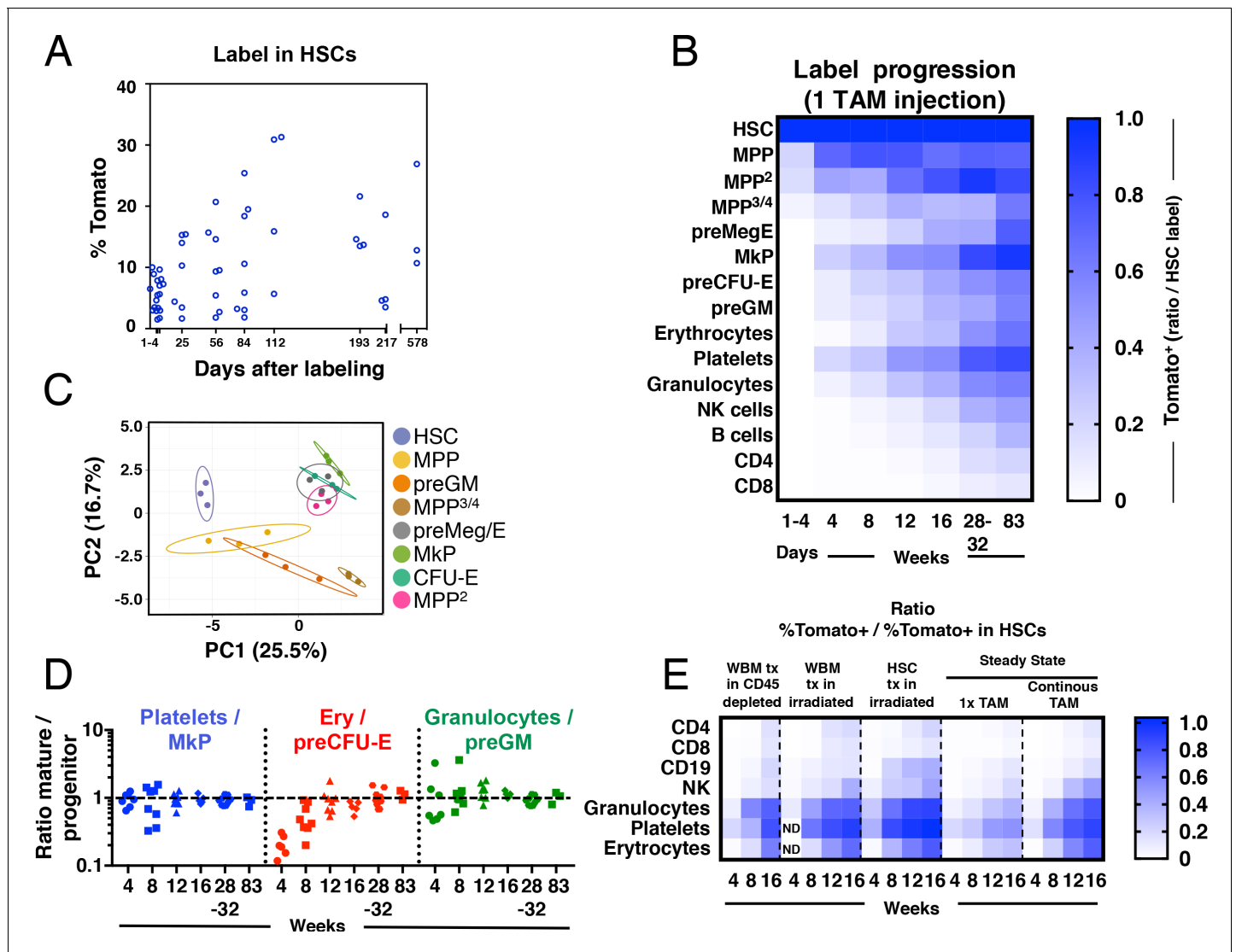
Figure 2. Fgd5-CreERT2 mediated lineage tracing reveals robust HSC contribution with distinct kinetics into hematopoietic cell subsets in steady state and after transplantation. Cohorts of *Fgd5*^CreERT2/+^; *Rosa26*^lsl-Tomato/+^ mice were chased for up to 83 weeks after receiving one Tamoxifen injection before endpoint analysis of the % of Tomato$^+$ cells in HSCs (A) and hematopoietic progenitor and PB cell subsets (B). The fraction of Tomato$^+$ cells in each indicated hematopoietic cell subset was divided by the % Tomato label in HSCs in corresponding mice to determine the ratio of Tomato$^+$ cells relative to HSCs in individual mice. The average ratio is plotted according to time after the Tamoxifen (TAM) injection and displayed in a heat map format. Mice were analyzed at 1–4 days (n = 18) and at 4 (n = 7), 8 (n = 8), 12 (n = 8), 16 (n = 4), 28 (n = 4), 32 (n = 5) and 83 (n = 3) weeks after the Tamoxifen injection. All mice were between 5 and 11 weeks old at the time of Tamoxifen injection. (C) PCA plot of multiplexed qRT-PCR data for 48 genes from triplicates of 10 cells from each of the indicated populations. Ellipses show an area where a new observation from the same group would position itself with a probability of 0.95. Numbers indicate the % of variance in the total data set that the respective PC explains. (D) For individual animals, the % of Tomato$^+$ cells in PB cell types was divided by the % of Tomato$^+$ cells in the indicated progenitor cell types and this value was plotted according to the duration of the chase period. Symbols represent individual mice (number of mice analyzed as in A and B). A dashed line is drawn to indicate an equilibrium-ratio of 1. (E) Ratios calculated as in B and plotted according to the number of weeks after transplantation or after the start of Tamoxifen administration for steady state/native mice (n = 3 for WBM tx in CD45 depleted, n = 5 for WBM tx in irradiated, n = 11 for HSC tx in irradiated, n = 4–8 for 1x TAM, n = 4–9 for continous TAM). All *Fgd5*^CreERT2/+^; *Rosa26*^lsl-Tomato/+^ mice/cells were between 5 and 11 weeks old at the time of Tamoxifen administration or when used as cell donors for transplantation.

The following figure supplements are available for figure 2:

Figure supplement 1. Label induction and progression in 1x Tamoxifen treated adult *Fgd5*^CreERT2/+^; *Rosa26*^lsl-Tomato/+^ mice.

Figure supplement 2. In vitro differentiation potential of LSK HSPCs.

Figure 2 continued on next page

Of the distinct progenitor fractions within the Lin⁻kit⁺ fraction (*Figure 1—figure supplement 1A*), megakaryocyte progenitors (MkP) acquired label with the fastest kinetics, reaching label equilibrium with HSCs after 32 weeks. Other myeloerythroid progenitors, including pre-megakaryocytic/erythroid (preMeg/E), pre-colony forming unit-erythroid (pre CFU-E) and pre-granulocyte-macrophage (preGM) progenitors acquired Tomato label with very similar kinetics despite their distinct lineage affiliations, although they never quite reached an equilibrium with HSCs throughout the course of the experiments (*Figure 2B* and *Figure 2—figure supplement 1*).

Mature effector cells represent the terminal progeny of HSCs. We observed distinct generation kinetics for different lineages (*Figure 2B*). First, we made the general observation that myeloerythroid cells acquired label more rapidly than lymphoid cells. Among the myeloid subsets, platelets acquired Tomato label with the fastest kinetics, followed by granulocytes and erythrocytes. Among lymphoid cell types, NK cells displayed faster labeling kinetics followed by B cells. T cells showed the slowest labeling kinetics among lymphoid cells and CD4⁺ T cells acquired label faster than CD8⁺ T cells (*Figure 2B*). Because the frequency of Tomato⁺ cells increased over time in all evaluated lineages, this data demonstrate a continuous contribution of HSCs to all hematopoietic lineages.

While multiple studies have defined populations of hematopoietic progenitors that associate with distinct developmental and/or stages of differentiation (*Bryder et al., 2006*), it is unknown whether such described progenitors are obligatory intermediates and/or their quantitative association relative to their anticipated mature offspring. Therefore, we interrogated the relationships between the rates of (re)generation of candidate committed myeloerythroid progenitors to those of their proposed mature cell lineage. At the earliest time points evaluated, we observed for all evaluated fractions a higher label in their corresponding progenitors (*Figure 2D*). However, this was resolved during the course of the experiments and reached similar equilibrium ratios for all evaluated lineages, although the erythroid lineage displayed somewhat slower kinetics (*Figure 2D*). Collectively, these experiments are in line with the view that progenitor generation precedes the generation of mature cells and that previously proposed progenitors appears to be, at least for the most part, obligatory intermediates.

Hematopoiesis after transplantation of HSCs is fundamentally different from unperturbed hematopoiesis (*Busch et al., 2015*; *Sun et al., 2014*). However, to what extent the pre-conditioning regimen and co-transplantation of mature cells and progenitors influence on hematopoiesis from HSCs is less established. Therefore, we next transplanted wild type recipient mice on continuous Tamoxifen diet with purified *Fgd5^{CreERT2/+}*; *Rosa26^{lsl-Tomato/+}* HSCs or WBM cells. Here, recipient mice were pre-conditioned by either lethal irradiation or antibody mediated CD45-depletion (*Palchaudhuri et al., 2016*). Due to the HSC specificity of the model, this approach allowed us to monitor the kinetics of the HSC contribution to all lineages after transplantation and compare it to the HSC contribution in steady state (*Figure 2E*). Compared to steady state, label progression in transplanted mice were faster (*Figure 2E*). When label progression kinetics was compared between HSC and WBM transplanted animals, HSC transplantation resulted in faster label progression, especially into the B cell lineage (*Figure 2E*). This likely reflects a significant contribution to the regeneration of the B cell lineage by co-transplanted long-lived B-lineage progenitors and mature cells after WBM transplantation. Comparison of label progression after WBM transplantation into irradiated or non-irradiated/antibody-mediated conditioned recipient mice revealed similar label progression kinetics into most mature lineages, with the exception of platelets that displayed a faster label progression in irradiated mice. This suggests that progenitors for platelets are more effectively ablated by irradiation than antibody-mediated pre-conditioning.

Fgd5-mediated HSC lineage tracing corroborates the fetal/juvenile origin of Langerhans cells, B1a B cells and brain microglial cells

While a labeling regimen of one Tamoxifen injection allows for accurate kinetic evaluations (*Figure 2A–B,D*), this experimental strategy labels only a fraction of HSCs (*Figure 1E* and *Figure 2A*) and thus necessitates correlation of label in HSCs to other evaluated cell subsets

(*Busch et al., 2015*) (*Figure 2B*). If the original HSC label is low, this might as a consequence not allow for evaluation of the activity of the entire pool of HSCs.

To explore whether we could label the HSC pool more extensively, *Fgd5*[CreERT2/+]; *Rosa26*[lsl-Tomato/+] mice were fed Tamoxifen containing food pellets for 16 weeks. To rule out adverse effects of prolonged Tamoxifen treatment on HSC proliferation, these experiments were preceded by a control label retaining experiment using *Col1a1*[tetO-H2B-mCherry/tetO-H2B-mCherry]; *ROSA26*[rtTA/rtT] mice (*Säwén et al., 2016*). Following H2B-mCherry induction with Doxycycline, mice were chased for 5 weeks in the presence or absence of Tamoxifen. Prolonged Tamoxifen treatment did not induce any additional proliferation within the HSC compartment, while more differentiated progenitors had readily proliferated in both settings (*Figure 3A*).

The 16 weeks labeling period was followed by an extensive (up to 41 weeks) chase period, during which mice received normal chow (*Figure 3B*). This labeling strategy resulted in labeling of virtually all candidate HSCs (*Figure 3C*). The blood of labeled mice was analyzed regularly to determine the fraction of Tomato^{+} cells in PB cell subsets (*Figure 1—figure supplement 1B*). Similar to after 1x Tamoxifen labeling, we observed robust label progression into all PB cell subsets, with similar kinetics in between different lineages (*Figure 3B*). However, a more complete HSC labeling resulted in a somewhat faster and more robust label progression into all PB cell subsets compared to 1x Tamoxifen labeling (*Figure 2E*). This was most evident for the lymphoid lineages, where the majority of PB cells had been generated from HSCs at the experiment end point upon prolonged Tamoxifen administration, whereas the ratio of labeled lymphocytes vs. labeled HSCs was low (>0,5) even after 83 weeks of chase in 1x Tamoxifen labeled mice (*Figure 2B*, *Figure 2E* and *Figure 3B*).

From endpoint mice in which the pool of HSCs was almost completely labeled (*Figure 3C*), we next interrogated the skin epidermis for Tomato[+] contribution to granulocytes and Langerhans cells. Granulocytes were almost completely Tomato positive, while Langerhans cells were devoid of label (*Figure 3D*, lower left), in line with the fetal origin and self-maintenance of the latter cells (*Collin and Milne, 2016*). Next, we interrogated Tomato expression in Vγ3δ^{+} T cells, an established fetal derived T cell subset (*Havran and Allison, 1990*). To our surprise, this revealed robust Tomato labeling of Vγ3δ^{+} T cells (*Figure 3D*, lower left). However, closer examination revealed high expression of ZsGreen in these cells (*Figure 3B*, lower middle). Therefore, rather than establishing adult contribution to this lineage, these experiments established Fgd5-CreERT2 transgene expression in Vγ3δ^{+} T cells.

B1a B cells represent an invariant subtype of B cells with a fetal origin that is primarily located in the peritoneum (*Hayakawa et al., 1985*), where they co-exists with more traditional B1b and B2 B cells in adult mice. While less than 10% of B1a B cells displayed Tomato label, around 50% of B1b B cells and the vast majority of B2 B cells (*Figure 3D* right) were Tomato[+] (comparable to levels in PB). This is in line with a more strict fetal/postnatal origin of B1a B cells, the ontogenically mixed origin of B1b B cells (*Kantor et al., 1995*) and an adult HSC origin of most B2 B cells.

Finally, we investigated adult HSC contribution to microglial cells of the brain, a subset of central nervous system myeloid cells that has been proposed to arise entirely from embryonic precursor cells (*Alliot et al., 1999*). Evaluations by confocal microscopy of the brain parenchyma revealed no detectable Tomato expression in IBA-1^{+} microglia (*Figure 3E*), while Fgd5 expressing endothelial cells (*Cheng et al., 2012*; *Gazit et al., 2014*) displayed abundant Tomato expression (*Figure 3E* middle).

Native hematopoiesis from HSCs declines with aging

We next set out to investigate how chronological aging influence on HSC contribution to hematopoiesis. To achieve rapid and robust labeling of HSCs, we labeled juvenile and aged *Fgd5*[CreERT2/+]; *Rosa26*[lsl-Tomato/+] mice by injecting Tamoxifen for five consecutive days (5x). Labeling was followed by evaluation of the fraction of Tomato positive cells in HSC and MPP fractions of the BM LSK compartment one day after the last Tamoxifen injection.

In aged mice, the initial labeling was highly specific to HSCs, with only low levels of labeling in MPP[2] cells. In sharp contrast, a larger fraction of LSKCD150^{-}CD48^{-} MPPs were labeled in juvenile mice (*Figure 4A*). Next, we correlated how increasing age influences on the HSC generation of other LSK/MPP subsets. *Fgd5*[CreERT2/+]; *Rosa26*[lsl-Tomato/+] mice between 6 and 96 weeks of age were labeled using a 5x Tamoxifen injection scheme, before evaluation of Tomato label in HSCs/MPP[2-4]21 days later. Ratios of the fraction of labeled MPPs vs. labeled HSCs in corresponding mice was
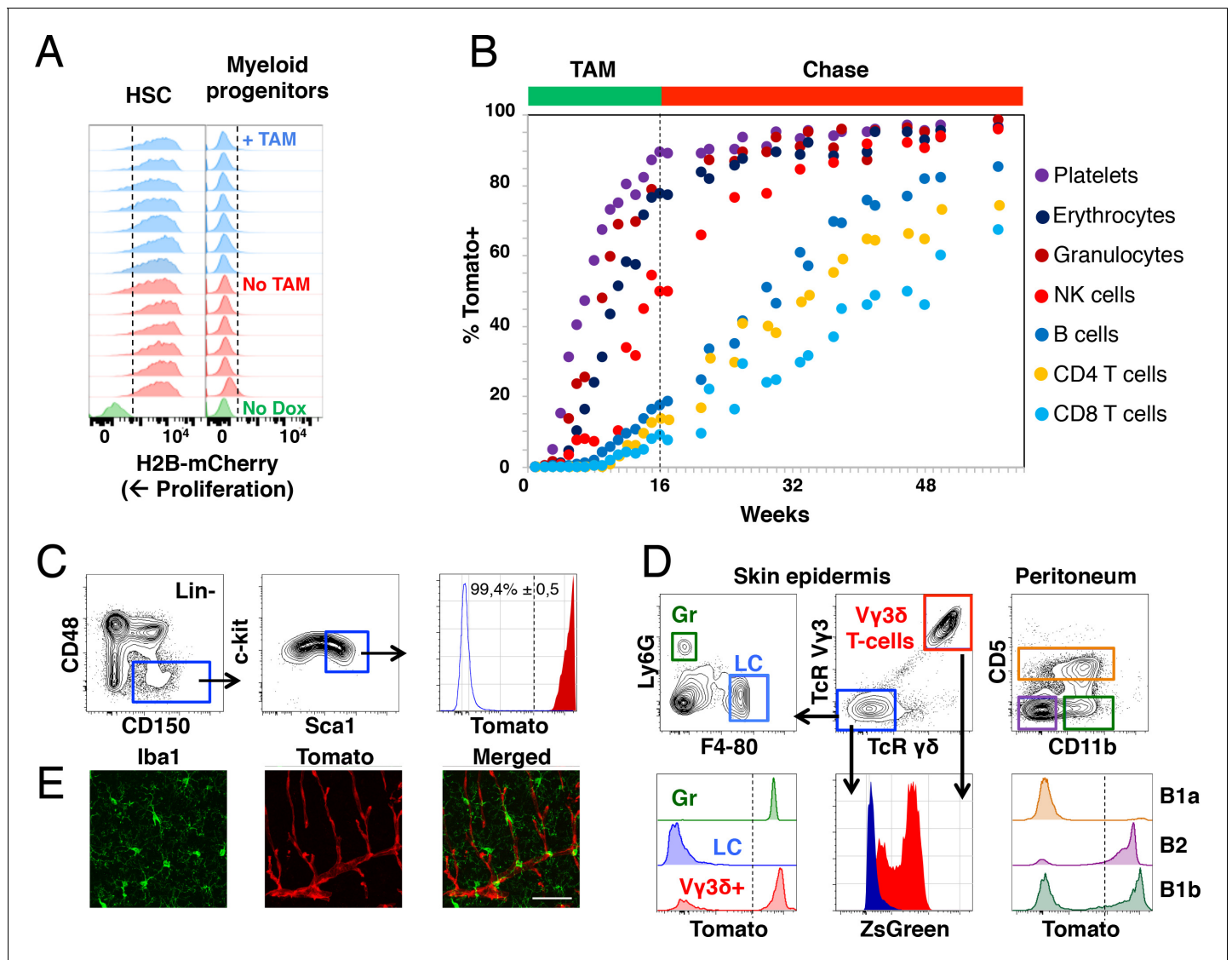
Figure 3. Fgd5-mediated lineage tracing after complete HSC labeling reveals limited adult HSCs contribution to tissue-resident immune cell subsets. (A) H2B-mCherry label retention in HSCs and myeloid progenitors after 5 weeks of chase in mice continuously fed Tamoxifen (TAM) containing food (blue histograms, n = 7) or normal food (red histograms, n = 6) during the chase period. Green histograms depict an unlabeled control. Dashed lines indicate the boundary for H2B-mCherry positivity. Lineage negative c-kit$^+$Sca1$^-$ cells are denoted as myeloid progenitors. (B) Cohorts of *Fgd5$^{CreERT2/+}$*; *Rosa26$^{lsl-Tomato/+}$* mice were continuously fed Tamoxifen food for 16 weeks (TAM phase) and thereafter normal chow during a chase phase of 32 weeks (n = 5) or 41 weeks (n = 4). During the TAM and chase phases, PB was regularly analyzed for Tomato label in the indicated subsets. Data points indicate the average % of Tomato label in each indicated subset. (C–E) Endpoint analysis, after 41 weeks chase, in mice from *Figure 3B* (n = 3). (C) Representative FACS plots showing the gating strategy to identify HSCs in lineage negative BM cells (left, middle) and depiction of the Tomato label in HSCs (right, red histogram) compared to an unlabeled control (blue histogram). Dashed line indicates the boundary for Tomato positivity, arrows indicate the gating strategy. (D) Representative FACS plots of cells isolated from skin tissue (epidermis) or the peritoneal cavity. Histograms show Tomato label (bottom left and right) or ZsGreen label (bottom middle) in the indicated subsets. Dashed line indicate the boundary for Tomato positivity, arrows indicate the gating hierarchy, gates and corresponding histograms are color matched. (E) Representative confocal images of the brain. (Left) IBA1 positive cells (green) are not labeled with Tomato (red, middle) while blood vessels are labeled with Tomato (middle). (Right) Merged images display both IBA1 staining and Tomato label. Scale bar = 50 μm. Mice in B-E were 5–6 weeks old at the start of Tamoxifen administration.
DOI: https://doi.org/10.7554/eLife.41258.008

calculated and plotted against mouse age at labeling (*Figure 4B*). This established that label progression into all MPP subsets in aged mice was substantially lower when compared to young adult mice and further revealed that the HSC contribution to MPPs and MPP$^{3/4}$s gradually declines with age towards very little replenishment of in particular MPP$^{3/4}$ in very old age (*Figure 4B*).
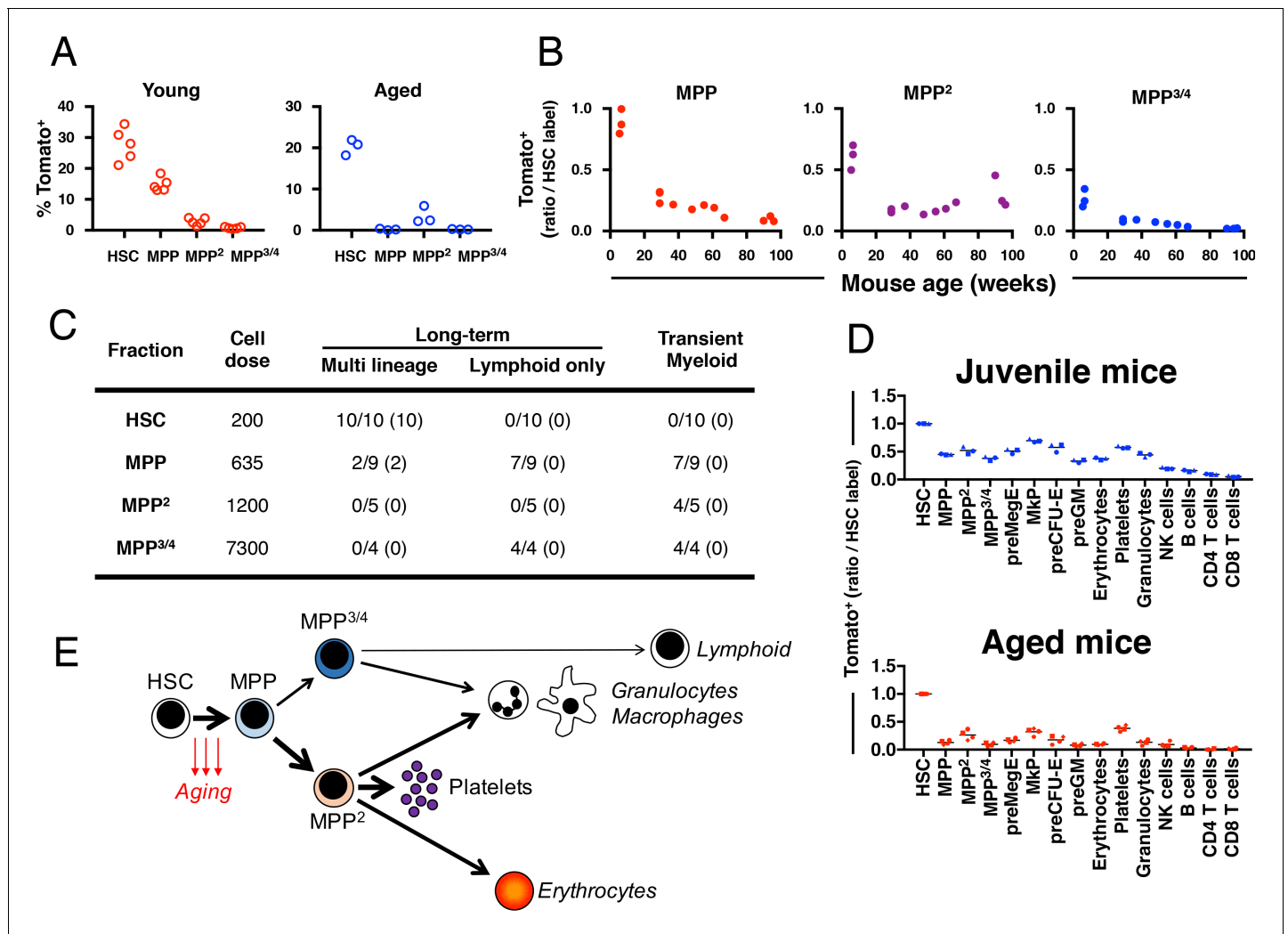
Figure 4. Fgd5 mediate lineage tracing reveals gradually declining HSC contribution to hematopoiesis with age. (**A**) Cohorts of aged (11–12 months; n = 3) or young (23–25 days; n = 5,) *Fgd5*[CreERT2/+]; *Rosa26*[lsl-Tomato/+] mice were injected with Tamoxifen 5 times on consecutive days and analyzed for Tomato label in LSK-HSPCs on day 6. Bars indicate median %. (**B**) *Fgd5*[CreERT2/+]; *Rosa26*[lsl-Tomato/+] mice were injected with Tamoxifen for 5 consecutive days and analyzed for Tomato label in LSK-HSPCs 21 days later. The % of Tomato+ cells in MPP[2-4] was divided by the % of Tomato+ HSCs in corresponding mice to determine the ratio of Tomato+ cells relative to HSCs. Ratios are plotted according to the age of mice at the time of Tamoxifen injection. (**C**) Indicated LSK subsets were isolated from *Fgd5*[CreERT2/+]; *Rosa26*[lsl-Tomato/+] mice and transplanted into WT mice on continuous Tamoxifen. Multilineage hematopoiesis and Tomato contribution was assed in PB 4, 8, 12 and 16 weeks after transplantation. Values in parenthesis indicate the number of mice with Tomato+ offspring. (**D**) Young (29 days; n = 3) and old (16 months; n = 4) *Fgd5*[CreERT2/+]; *Rosa26*[lsl-Tomato/+] mice were injected once with Tamoxifen and analyzed for Tomato label 18 weeks later. The % of Tomato+ cells in each indicated cell type was divided by the % of Tomato+ HSCs in corresponding mice to determine the ratio of Tomato+ cells relative to HSCs. (**E**) Model depicting HSC contribution to native hematopoiesis. Arrow weights and arrow lengths indicate the magnitude and the kinetics of HSC contribution to the indicated cell type respectively. The declining HSC contribution to hematopoiesis with age can be traced to a reduced differentiation of HSCs to MPPs (red arrows).

DOI: https://doi.org/10.7554/eLife.41258.009

The following figure supplement is available for figure 4:

Figure supplement 1. Aging associates with reduced multilineage HSC contribution.
DOI: https://doi.org/10.7554/eLife.41258.010

To evaluate the functional potential of initially Tomato-labeled MPPs, we FACS sorted HSCs and different MPP subsets isolated from non-labeled *Fgd5*[CreERT2/+]; *Rosa26*[lsl-Tomato/+] mice and transplanted cells into lethally irradiated wild type mice. Recipient mice were provided Tamoxifen containing food pellets throughout the experiment. We analyzed donor chimerism and Tomato labeled PB cells after repetitive PB blood sampling. As expected, we did not observe any multilineage long-

term reconstitution or Tomato$^+$ cells in MPP^2/MPP$^{3/4}$ transplanted mice (*Figure 4C*). 10 out of 10 HSC transplanted mice were multi lineage reconstituted at 16 weeks post transplantation with high levels of Tomato$^+$ donor cells in all evaluated lineages (*Figure 4C*). More surprisingly 2 out of 9 MPP transplanted mice displayed donor reconstitution levels > 1% in all lineages 16 weeks after transplantation (*Figure 4C*). This long-term multilineage reconstitution potential from MPPs was accompanied with robust Tomato labeling among donor cells and revealed that Tomato labeled phenotypic MPPs perform as bona fide HSCs after transplantation (*Figure 4C*). By contrast, mice that received MPP cells and displayed only transient myeloid reconstitution never displayed any Tomato$^+$ cells. This demonstrates, in young mice, the presence of a minor CD150$^-$ HSC activity that appears exclusively coupled to Fgd5 expression.

Finally, we were interested in determining whether the age-related decrease in HSC derived MPPs might influence on the generation kinetics of lineage-restricted progenitors and mature blood cells. For this, we labeled juvenile (29 days) and aged (87–89 weeks) *Fgd5*$^{CreERT2/+}$; *Rosa26*$^{lsl-Tomato/+}$ mice with 1x Tamoxifen, which was followed by evaluation of label progression after 18 weeks (*Figure 4D* and *Figure 4—figure supplement 1*). While the frequency of Tomato labeled HSCs was similar among the two groups (*Figure 4—figure supplement 1*), all progeny exhibited reduced frequencies of Tomato labeled cells in aged mice, demonstrating a strikingly reduced multilineage differentiation capacity of HSCs as a consequence of age.

Discussion

In this work, we explored the cellular contribution from HSCs using a HSC-specific lineage tracing approach. Our work revealed robust HSC contribution to adult multilineage hematopoiesis and, while not focused at studying fetal hematopoiesis, support the previously reported fetal/juvenile origins of several other specific hematopoietic subsets. We observed the fastest label progression into the platelet lineage, which might be related to the recent observations that at least a subset of HSCs appears platelet-biased (*Sanjuan-Pla et al., 2013*; *Shin et al., 2014*). Thereafter, erythrocytes and granulocytes acquired label with similar kinetics, although Tomato$^+$ erythrocytes emerged in the peripheral blood somewhat later than granulocytes. This likely reflects the slower turnover of mature erythrocytes compared to other myeloid cells. On the other hand, among granulocytes, we did not find any noticeable differences when evaluating HSC contribution to the neutrophil or eosinophil lineages (data not shown), despite the seemingly distinct transcriptional underpinnings of these lineages (*Drissen et al., 2016*).

Among lymphocytes, the HSC contribution was most rapid and robust to the NK cell lineage. At present, we can say little on whether this reflects an early and distinct progenitor intermediate for NK cells (*Wu et al., 2014*) or whether NK cells are, at least partially, regenerated through myeloid progenitors (*Chen et al., 2015*; *Grzywacz et al., 2011*). While the extremely slow HSC generation of adaptive immune components (and T cells in particular) have implications for our understanding of HSCs, by proposing that adult HSCs to a large extent present as myeloid-biased in an unperturbed scenario, our results also suggest the necessity of very harsh conditioning to achieve an 'immunological reboot' (the generation of naïve lymphocytes) in certain autoimmune situations (*Atkins et al., 2016*).

According to current models of hematopoiesis, lineage committed progenitors reside developmentally in between HSCs and their mature progeny, and much work has been aimed at detailing these stages (*Adolfsson et al., 2005*; *Akashi et al., 2000*; *Arinobu et al., 2007*; *Oguro et al., 2013*; *Pietras et al., 2015*; *Pronk et al., 2007*). What has remained more unknown is the relationships of these defined progenitors not only to HSCs and their mature offspring, but also whether they are obligatory. In our work, we could demonstrate that the generation rates of each evaluated myeloid progenitor subset correlated highly to their corresponding mature offspring, although the generation kinetics varied depending on lineage. Thus, although some challenges have recently been raised on how lineage commitment occur from HSCs based on inferences from large-scale single-cell RNA sequencing experiments (*Paul et al., 2015*; *Velten et al., 2017*), our data support the more conventional view that the generation of mature myeloid cells is preceded by the generation of obligatory lineage-committed intermediates.

Investigations of immature progenitors revealed that the most rapid label progression associated with LSKCD150$^-$CD48$^-$ MPPs. MPPs share many defining properties of HSCs, including multilineage

differentiation potential and very low proliferation rates in steady state (*Säwén et al., 2016*). The distinction of MPPs from HSCs is mainly thought to result from pronounced differences in self-renewal; a property so far entirely evaluated by transplantation. Intriguingly, our work revealed that LSKCD150-CD48- MPPs displayed more rapid label kinetics in young mice, which was gradually declining with advancing age. At the same time, we could in agreement with previous studies (*Weksberg et al., 2008*) also demonstrate a minor multilineage HSC activity in this compartment, which correlated exclusively to Fgd5 expression/Tomato labeling. Together with an overall decline in multilineage HSC contribution of aged mice, these results strongly propose a model in which aging associates with reduced/compromised HSC differentiation, which in combination with the well-established expansion of HSCs with age (*Morrison et al., 1996*; *Rossi et al., 2005*; *Sudo et al., 2000*) appears to represent a physiologically relevant compensatory mechanisms to sustain multilineage hematopoiesis from HSCs (*Figure 4E*).

Compared to MPPs, MPP$^{3/4}$ are perhaps easier to approach given their restrictions in lineage potential (lack of Meg/E potential) (*Adolfsson et al., 2005*; *Arinobu et al., 2007*; *Pietras et al., 2015*; *Pronk et al., 2007*). We found MPP$^{3/4}$ to be regenerated from HSCs with slow kinetics compared to other downstream myeloid progenitor cells, but also to MPP^2 cells, that we in agreement with other studies (*Pietras et al., 2015*) find 'primed' towards Meg/E development. Intriguingly, our data proposes a significant self-renewal activity of at least a subset of MPP$^{3/4}$, with the demonstration that this fraction never reached label equilibrium with HSCs in any evaluated experimental setting. This might be particularly relevant in the setting of age, a situation in which HSC was found to generate MPP$^{3/4}$ very inefficiently (*Figure 4E*).

While limited, a few groups have recently approached HSC contribution to native hematopoiesis. Evaluations of hematopoiesis using transposon mobilization led to the conclusion that HSCs are not major contributors to adult hematopoiesis (*Sun et al., 2014*). To some degree, this conclusion was later corroborated by CreER-mediated labeling of a minor fraction of the adult HSC pool using a Tie2-based CreER driver (*Busch et al., 2015*). Limited HSC contribution to adult hematopoiesis is in sharp contrast to the results we present here and to results from another recent study (*Sawai et al., 2016*). Our studies would propose that absence of a HSC specific driver, as in the work from Sun et al., makes interpretations of HSC contribution very complicated, not the least for the lymphoid lineages, while the labeling of only a minor fraction of HSCs, as in the work from Busch et al., might select for a subset of HSCs with a rather distinct functional behavior.

In summary, we conclude that although the study of native hematopoiesis highlights fundamental differences, with in particular slower regeneration times from HSCs to those seen after transplantation, they regardless corroborate decades of research derived from transplantation experiments in which HSCs has been proposed to continuously contribute to hematopoiesis.

Materials and methods

Key resources table

Reagent type (species) or resource	Designation	Source or reference	Identifiers	Additional information
Strain, strain background (M. musculus)	*Fgd5-CreERT2*	PMID:24958848	RRID:IMSR_JAX:027789	
Strain, strain background (M. musculus)	*Rosa26-rtTA; Col1a1-tetO-H2B-mCherry*	PMID:17554301	RRID:IMSR_JAX:014602	
Strain, strain background (M. musculus)	*Rosa26-Lox-Stop-Lox-Tomato*	PMID:20023653	RRID:IMSR_JAX:007905	
Antibody	B220 PECy5 Clone: RA3-6B2	Biolegend	RRID:AB_312994	(1:400)

Continued on next page

Continued

Reagent type (species) or resource	Designation	Source or reference	Identifiers	Additional information
Antibody	B220 biotin	Biolegend	RRID:AB_312989	(1:200)
	Clone: RA3-6B2			
Antibody	B220 APC	Biolegend	RRID:AB_312997	(1:400)
	Clone: RA3-6B2			
Antibody	CD105 PECy7	Biolegend	RRID:AB_1027700	(1:200)
	Clone: MJ7/18			
Antibody	CD115 BV605	Biolegend	RRID:AB_2562760	(1:200)
	Clone: CSF-1R			
Antibody	CD11b PECy5	Biolegend	RRID:AB_312793	(1:400)
	Clone: M1/70			
Antibody	CD11b biotin	Biolegend	RRID:AB_312787	(1:200)
	Clone: M1/70			
Antibody	CD11b APC	Biolegend	RRID:AB_312795	(1:800)
	Clone: M1/70			
Antibody	CD11b APC-Cy7	Biolegend	RRID:AB_830641	(1:200)
	Clone: M1/70			
Antibody	CD11c BV570	Biolegend	RRID:AB_10900261	(1:200)
	Clone: N418			
Antibody	CD150 APC	Biolegend	RRID:AB_493460	(1:400)
	Clone: TC15-12F12.2			
Antibody	CD150 PE	Biolegend	RRID:AB_313683	(1:200)
	Clone: TC15-12F12.2			
Antibody	CD16/32 AL700	eBioscience	RRID:AB_493994	(1:100)
	Clone: 93			
Antibody	CD19 PECy7	eBioscience	RRID:AB_657663	(1:200)
	Clone: 1D3			
Antibody	CD19 BV-786	BD-Horizon	RRID:AB_2738141	(1:200)
	Clone: 1D3			
Antibody	CD25 APC	eBioscience	RRID:AB_469366	(1:100)
	Clone: PC 61.5			
Antibody	CD31 PerCpCy5.5	Biolegend	RRID:AB_2566761	(1:200)
	Clone: MEC13.3			
Antibody	CD3e PECy5	Biolegend	RRID:AB_312675	(1:400)
	Clone: 145–2 C11			
Antibody	CD3e biotin	Biolegend	RRID:AB_2563947	(1:200)
	Clone: 17A2			
Antibody	CD3 AL700	Biolegend	RRID:AB_493697	(1:200)
	Clone: 17A2			

Continued

Reagent type (species) or resource	Designation	Source or reference	Identifiers	Additional information
Antibody	CD4 BV711	Biolegend	RRID:AB_2562607	(1:200)
	Clone: RM4-5			
Antibody	CD4 APC eFl780	eBioscience	RRID:AB_1272219	(1:200)
	Clone: RM4-5			
Antibody	CD41 PerCP-eFl710	eBioscience	RRID:AB_10855042	(1:200)
	Clone: MWReg30			
Antibody	CD45.1 AL700	Biolegend	RRID:AB_493733	(1:200)
	Clone: A20			
Antibody	CD45.2 PECy7	Biolegend	RRID:AB_1186098	(1:200)
	Clone: 104			
Antibody	CD45.2 PE/Dazzle	Biolegend	RRID:AB_2564177	(1:200)
	Clone: 104			
Antibody	CD45.2 BV785	Sony	RRID:AB_2562604	(1:200)
	Clone: 104			
Antibody	CD45.2 biotin	Biolegend	RRID:AB_313441	(1:200)
	Clone: 104			
Antibody	CD48 PECy7	Biolegend	RRID:AB_2075049	(1:200)
	Clone: HM48-1			
Antibody	CD48 AL700	Biolegend	RRID:AB_10612755	(1:200)
	Clone: HM48-1			
Antibody	CD5 BV-421	BD-Horizon	RRID:AB_2737758	(1:200)
	Clone: 53–7.3			
Antibody	CD8 PerCpCy5.5	Sony	RRID:AB_2075239	(1:200)
	Clone: 53–6.7			
Antibody	c-kit APCeFl780	eBioscience	RRID:AB_1272177	(1:200)
	Clone: 2B8			
Antibody	c-kit APC	Biolegend	RRID:AB_313221	(1:100)
	Clone: 2B8			
Antibody	F4/80 BV421	Biolegend	RRID:AB_11203717	(1:200)
	Clone: BM8			
Antibody	Flt3 biotin	eBioscience	RRID:AB_466600	(1:200)
	Clone: AZF10			
Antibody	Gr1 PECy5	Biolegend	RRID:AB_313375	(1:400)
	Clone: RB6-8C5			
Antibody	Gr1 FITC	BD PH	RRID:AB_394643	(1:400)
	Clone: RB6-8C5			
Antibody	Gr1 biotin	Biolegend	RRID:AB_313369	(1:200)
	Clone: RB6-8C5			

Continued on next page

Continued

Reagent type (species) or resource	Designation	Source or reference	Identifiers	Additional information
Antibody	Gr1 BV711	Sony	RRID:AB_2562549	(1:200)
	Clone: RB6-8C5			
Antibody	IL7Ra BV510	Sony	RRID:AB_2564576	(1:200)
	Clone: A7R34			
Antibody	Ly6G APC/Fire750	Biolegend	RRID:AB_2616733	(1:200)
	Clone: 1A8			
Antibody	NK1.1 PECy5	Biolegend	RRID:AB_493591	(1:400)
	Clone: PK136			
Antibody	NK1.1 Pacific Blue	Biolegend	RRID:AB_2132712	(1:200)
	Clone: PK136			
Antibody	Sca1 Pacific Blue	Biolegend	RRID:AB_2143237	(1:200)
	Clone: E13-161.7			
Antibody	TcR Vγ3 APC	Biolegend	RRID:AB_10895900	(1:200)
	Clone: 536			
Antibody	TcR γ/δ BV605	Biolegend	RRID:AB_2563356	(1:200)
	Clone: GL3			
Antibody	Ter119 PECy5	Biolegend	RRID:AB_313711	(1:400)
	Clone: Ter-119			
Antibody	Ter119 biotin	Biolegend	RRID:AB_313705	(1:200)
	Clone: Ter-119			
Antibody	Ter119 PerCpCy5.5	Biolegend	RRID:AB_893636	(1:200)
	Clone: Ter-119			
Peptide, recombinant protein	Streptavidin BV605	Biolegend		(1:400)
Peptide, recombinant protein	Streptavidin-Saporin	PMID: 27272386 Advanced Targeting Systems		
Chemical compound, drug	Tamoxifen	Sigma-Aldrich	I.p. 50 mg/kg	
Chemical compound, drug	Doxycycline	Ssniff Spezialdiäten	Food 2 g/kg	
Chemical compound, drug	Tamoxifen	Ssniff Spezialdiäten	Food 400 mg/kg Tamoxifen Citrate	
Software, algorithm	Flowjo	FlowJo (https://www.flowjo.com/solutions/flowjo)	RRID:SCR_008520	

Continued on next page

Continued

Reagent type (species) or resource	Designation	Source or reference	Identifiers	Additional information
Software, algorithm	Microsoft Excel	Microsoft Excel (https://www.microsoft.com/en-gb/)	RRID: SCR_016137	
Software, algorithm	Graphpad Prism	GraphPad Prism (https://graphpad.com)	RRID: SCR_002798	

Mouse procedures

For inducible marking of HSCs in vivo, we crossed *Fgd5-2A-ZsGreen-CreERT2* mice (*Gazit et al., 2014*) (JAX 027789) to *Rosa26-LoxP-Stop-LoxP-Tomato* (*Madisen et al., 2010*) (JAX 007905) mice, resulting in *Fgd5$^{CreERT2/+}$; Rosa26$^{lsl-Tomato/+}$* mice. For simultaneous in vivo tracking of proliferation history and marking of HSCs, *Fgd5$^{CreERT2/+}$; Rosa26$^{lsl-Tomato/+}$* mice were crossed with *Col1a1$^{tetO-H2B-mCherry/tetO-H2B-mCherry}$; ROSA26$^{rtTA/rtTA}$* mice (JAX 014602) to generate *Fgd5$^{CreERT2/+}$; Rosa26$^{lsl-Tomato/rtTA}$; Col1a1$^{tetO-H2B-mCherry/+}$*. Such mice were administered doxycycline in food pellets (2 g/kg; Ssniff Spezialdiäten) for 2 weeks followed by 5 weeks of chase before HSC marking by a single i.p. Tamoxifen injection (50 mg/kg) and analysis 5 days later.

Tamoxifen was purchased from Sigma-Aldrich and suspended at 100 mg/ml in ethanol and mixed with sunflower oil to a concentration of 10 mg/ml. Tamoxifen was administered by intraperitoneal injections at 50 mg/kg body weight once (1x) or for 5 (5x) consecutive days. To acquire full/maximal HSC labeling, cohorts of mice were continuously fed Tamoxifen containing food pellets for 16 weeks. Mice on Tamoxifen food were regularly bled (sparsely; 1–2 drops) during the labeling period and during the chase period.

Transplanted recipient mice were subjected to lethal irradiation (950 rad) except CD45.1/2 mice that were CD45-depleted by intravenous injection of an immunotoxin (3 mg/kg) consisting of CD45.2-biotin (clone 104) and streptavidin-Saporin (Advanced Targeting Systems) in a 1:1 molar ratio 3 days prior to transplantation, as described (*Palchaudhuri et al., 2016*). All transplanted cells were isolated from CD45.2 *Fgd5$^{CreERT2/+}$; Rosa26$^{lsl-Tomato/+}$* mice. CD45-depleted recipients were transplanted with 10^7 whole bone marrow (WBM) cells and irradiated mice were transplanted with 3 $\times$ 10^6 WBM cells (n = 7), 200 (n = 10) or 100 (n = 2) HSCs, 635 MPPs (n = 10), 1200 MPP^{2}s (n = 5) or 7300 MPP$^{3/4}$s (n = 4). Tomato$^+$ and Tomato$^-$ HSCs were isolated from *Fgd5$^{CreERT2/+}$; Rosa26$^{lsl-Tomato/+}$* mice injected with Tamoxifen 2 days before isolation and transplantation into congenic C57BL/6 (CD45.1$^+$) mice on normal chow. Before transplantations of HSCs or MPPs FACS sorted cells were mixed with 3 $\times$ 10^5 WBM competitor cells in 200 µl PBS supplemented with 2 mM EDTA and 2% FBS before injection. Where indicated, recipient mice were given Tamoxifen containing food pellets (400 mg/kg Tamoxifen Citrate, Ssniff Spezialdiäten) throughout the experiments. At the indicated time point, PB was collected from the tail vein for reconstitution analysis.

H2B-mCherry labeling in *Col1a1$^{tetO-H2B-mCherry/tetO-H2B-mCherry}$; ROSA26$^{rtTA/rtTA}$* mice was induced by administration of doxycycline (*Säwén et al., 2016*). Thereafter, mice were chased for 5 weeks while eating Tamoxifen containing food pellets or normal chow (No TAM), followed by FACS analysis to assess H2B-mCherry dilution in HSCs/progenitors.

All mice were maintained at the animal facilities at BMC at Lund University and all experiments were performed with consent from the Malmö/Lund animal ethics board, reference number M186-15.

Immunophenotyping and FACS

Immunophenotyping by FACS was done as described (*Säwén et al., 2016*) (*Supplementary file 1*). For platelet and erythrocyte analysis, 1 µl of whole blood was taken to 300 µl PBS before FACS analysis. Cells were sorted and/or analyzed on a FACS Aria III cell sorter (Becton Dickinson) or on a LSRFortessa (Becton Dickinson).

B1a, Langerhans cells and Vg3^{+} T cell analysis

For isolation of peritoneal cells, peritoneal lavage was performed using 10 mL PBS. For isolation of skin epidermal cells, the flank of the mouse was shaved before excision of skin. The skin was incubated for 25 min at 37°C in a dissociation buffer (PBS containing 2.4 mg/ml of dispase (Roche) and 3% FCS) before separation of dermis from the epidermis. Pieces of epidermis were incubated for 30 min at 37°C in digestion buffer (PBS supplemented with 1 mg/ml collagenase IV [Sigma-Aldrich], 100 U/ml DNase I [Sigma], 2.4 mg/ml dispase [Roche] and 3% FBS) and thereafter filtered and stained against indicated markers. Before analysis, cells were incubated with Propidium Iodide (Invitrogen) to exclude dead cells.

Immunohistochemistry

Mice were deeply anaesthetized with an overdose of pentobarbital and transcardially perfused with cold saline. Brains were post-fixed for 48 hr in 4% paraformaldehyde (PFA) and incubated in 20% sucrose for 24 hr before being cut in 30 µm thick coronal sections on a microtome. Sections were incubated in blocking solution (5% normal serum and 0.25% Triton X-100 in 0.1 M potassium-phosphate buffered solution) for one hour and subsequently overnight at 4°C with the primary antibody (Iba1 1:1000 Wako). Fluorophore-conjugated secondary antibody (Molecular Probes or Jackson Laboratories) was diluted in blocking solution and applied for 2 hr at room temperature. Tomato label could be detected without any staining. Nuclei were stained with Hoechst (Molecular Probes) for 10 min and sections were mounted with Dabco mounting medium. Images were obtained using confocal microscopy (Zeiss, Germany).

Cell culture

Single LSKCD150^{+}CD48^{+} cells, MPP[3/4]s and HSCs were sorted into Terasaki wells containing 20 µl of media (OptiMEM supplemented with 10% FCS, 1:1000 Gentamicin (Invitrogen), 1:100 GlutaMAX (Invitrogen) and 1:500 β-mercaptoethanol (Invitrogen) supplemented with cytokines (mSCF (Peprotech) 100 ng/ml, TPO (Peprotech) 10 ng/ml, IL-3 (Peprotech) 5 ng/ml, EPO (Janssen) 5units/ml, human G-CSF (Amgen) 10 ng/ml). After 6 days of culture at 37°C, wells were scored and evaluated for the presence of megakaryocytes and erythroid cells by visual inspection in microscope.

Gene expression analyses

qRT-PCR analyses using the Fluidigm Biomark HD Platform was done as described (*Säwén et al., 2016*) (*Supplementary file 2*). PCA on gene expression data from all reference populations was performed using Clustvis, (http://biit.cs.ut.ee/clustvis/).

Single-cell RNA seq libraries were generated using a Chromium system (10x Genomics) according to the manufacturer's instructions. Two consecutive sequencing runs were performed to achieve enough sequencing depth and data was combined and further analyzed using the Cell Ranger[TM] pipeline (10x Genomics). The accession number for the single-cell RNA sequencing data reported in this paper is GSE122473.

Statistical analysis

Data were analyzed using Microsoft Excel (Microsoft) and Graphpad Prism (GraphPad Software). All FACS analyses were performed using Flowjo software (TreeStar).

Additional information

Author contributions

Petter Säwen, Conceptualization, Formal analysis, Validation, Investigation, Visualization, Methodology, Writing—original draft, Project administration, Writing—review and editing; Mohamed Eldeeb, Investigation; Eva Erlandsson, Trine A Kristiansen, Zaal Kokaia, Joan Yuan, Methodology; Cecilia Laterza, Investigation, Methodology; Göran Karlsson, Formal analysis, Methodology; Shamit Soneji, Data curation, Formal analysis; Pankaj K Mandal, Derrick J Rossi, Resources; David Bryder, Conceptualization, Resources, Formal analysis, Supervision, Funding acquisition, Visualization, Writing—original draft, Project administration, Writing—review and editing

Author ORCIDs

Petter Säwen (iD) http://orcid.org/0000-0001-6854-1434
Zaal Kokaia (iD) http://orcid.org/0000-0003-2296-2449
David Bryder (iD) http://orcid.org/0000-0002-8761-4237

Ethics

Animal experimentation: All mice were maintained at the animal facilities at BMC at Lund University, and were performed with consent from a local ethical committee reference number M186-15

Decision letter and Author response

Decision letter https://doi.org/10.7554/eLife.41258.017
Author response https://doi.org/10.7554/eLife.41258.018

Additional files

Supplementary files

• Supplementary file 1. Definitions of cells used throughout study.
DOI: https://doi.org/10.7554/eLife.41258.011

• Supplementary file 2. List of analyzed genes in mutiplexed qRT-PCR gene expression analyses (*Figure 2C*).
DOI: https://doi.org/10.7554/eLife.41258.012

• Transparent reporting form
DOI: https://doi.org/10.7554/eLife.41258.013

Data availability

Sequencing data have been deposited in GEO under accession code GSE122473.

The following dataset was generated:

			Database and

Author(s)	Year	Dataset title	Dataset URL	Identifier
Säwén P, Erlands-son E, Soneji S, Bryder D	2018	HSCs contribute actively to native multilineage hematopoiesis but with reduced differentiation capacity upon aging	https://www.ncbi.nlm. nih.gov/geo/query/acc. cgi?acc=GSE122473	Gene Expression Omnibus, GSE122473

References

Acar M, Kocherlakota KS, Murphy MM, Peyer JG, Oguro H, Inra CN, Jaiyeola C, Zhao Z, Luby-Phelps K, Morrison SJ. 2015. Deep imaging of bone marrow shows non-dividing stem cells are mainly perisinusoidal. *Nature* **526**: 126–130. DOI: https://doi.org/10.1038/nature15250, PMID: 26416744

Adolfsson J, Månsson R, Buza-Vidas N, Hultquist A, Liuba K, Jensen CT, Bryder D, Yang L, Borge OJ, Thoren LA, Anderson K, Sitnicka E, Sasaki Y, Sigvardsson M, Jacobsen SE. 2005. Identification of Flt3+ lympho-myeloid stem cells lacking erythro-megakaryocytic potential a revised road map for adult blood lineage commitment. *Cell* **121**:295–306. DOI: https://doi.org/10.1016/j.cell.2005.02.013, PMID: 15851035

Akashi K, Traver D, Miyamoto T, Weissman IL. 2000. A clonogenic common myeloid progenitor that gives rise to all myeloid lineages. *Nature* **404**:193–197. DOI: https://doi.org/10.1038/35004599, PMID: 10724173

Alliot F, Godin I, Pessac B. 1999. Microglia derive from progenitors, originating from the yolk sac, and which proliferate in the brain. *Developmental Brain Research* **117**:145–152. DOI: https://doi.org/10.1016/S0165-3806 (99)00113-3, PMID: 10567732

Arinobu Y, Mizuno S, Chong Y, Shigematsu H, Iino T, Iwasaki H, Graf T, Mayfield R, Chan S, Kastner P, Akashi K. 2007. Reciprocal activation of GATA-1 and PU.1 marks initial specification of hematopoietic stem cells into myeloerythroid and myelolymphoid lineages. *Cell Stem Cell* **1**:416–427. DOI: https://doi.org/10.1016/j.stem. 2007.07.004, PMID: 18371378

Atkins HL, Bowman M, Allan D, Anstee G, Arnold DL, Bar-Or A, Bence-Bruckler I, Birch P, Bredeson C, Chen J, Fergusson D, Halpenny M, Hamelin L, Huebsch L, Hutton B, Laneuville P, Lapierre Y, Lee H, Martin L, McDiarmid S, et al. 2016. Immunoablation and autologous haemopoietic stem-cell transplantation for aggressive multiple sclerosis: a multicentre single-group phase 2 trial. *The Lancet* **388**:576–585. DOI: https:// doi.org/10.1016/S0140-6736(16)30169-6

Bando JK, Colonna M. 2016. Innate lymphoid cell function in the context of adaptive immunity. *Nature Immunology* **17**:783–789. DOI: https://doi.org/10.1038/ni.3484, PMID: 27328008

Benz C, Copley MR, Kent DG, Wohrer S, Cortes A, Aghaeepour N, Ma E, Mader H, Rowe K, Day C, Treloar D, Brinkman RR, Eaves CJ. 2012. Hematopoietic stem cell subtypes expand differentially during development and display distinct lymphopoietic programs. *Cell Stem Cell* **10**:273–283. DOI: https://doi.org/10.1016/j.stem.2012. 02.007, PMID: 22385655

Biasco L, Pellin D, Scala S, Dionisio F, Basso-Ricci L, Leonardelli L, Scaramuzza S, Baricordi C, Ferrua F, Cicalese MP, Giannelli S, Neduva V, Dow DJ, Schmidt M, Von Kalle C, Roncarolo MG, Ciceri F, Vicard P, Wit E, Di Serio C, et al. 2016. In Vivo tracking of human hematopoiesis reveals patterns of clonal dynamics during early and steady-state reconstitution phases. *Cell Stem Cell* **19**:107–119. DOI: https://doi.org/10.1016/j.stem.2016.04. 016, PMID: 27237736

Bowie MB, Kent DG, Dykstra B, McKnight KD, McCaffrey L, Hoodless PA, Eaves CJ. 2007. Identification of a new intrinsically timed developmental checkpoint that reprograms key hematopoietic stem cell properties. *PNAS* **104**:5878–5882. DOI: https://doi.org/10.1073/pnas.0700460104, PMID: 17379664

Bryder D, Rossi DJ, Weissman IL. 2006. Hematopoietic stem cells: the paradigmatic tissue-specific stem cell. *The American Journal of Pathology* **169**:338–346. DOI: https://doi.org/10.2353/ajpath.2006.060312, PMID: 16 877336

Busch K, Klapproth K, Barile M, Flossdorf M, Holland-Letz T, Schlenner SM, Reth M, Höfer T, Rodewald HR. 2015. Fundamental properties of unperturbed haematopoiesis from stem cells in vivo. *Nature* **518**:542–546. DOI: https://doi.org/10.1038/nature14242, PMID: 25686605

Chen Q, Ye W, Jian Tan W, Mei Yong KS, Liu M, Qi Tan S, Loh E, Te Chang K, Chye Tan T, Preiser PR, Chen J. 2015. Delineation of natural killer cell differentiation from myeloid progenitors in human. *Scientific Reports* **5**: 15118. DOI: https://doi.org/10.1038/srep15118, PMID: 26456148

Chen JY, Miyanishi M, Wang SK, Yamazaki S, Sinha R, Kao KS, Seita J, Sahoo D, Nakauchi H, Weissman IL. 2016. Hoxb5 marks long-term haematopoietic stem cells and reveals a homogenous perivascular niche. *Nature* **530**: 223–227. DOI: https://doi.org/10.1038/nature16943, PMID: 26863982

Cheng C, Haasdijk R, Tempel D, van de Kamp EH, Herpers R, Bos F, Den Dekker WK, Blonden LA, de Jong R, Bürgisser PE, Chrifi I, Biessen EA, Dimmeler S, Schulte-Merker S, Duckers HJ. 2012. Endothelial cell-specific FGD5 involvement in vascular pruning defines neovessel fate in mice. *Circulation* **125**:3142–3159. DOI: https:// doi.org/10.1161/CIRCULATIONAHA.111.064030, PMID: 22661514

Collin M, Milne P. 2016. Langerhans cell origin and regulation. *Current Opinion in Hematology* **23**:28–35. DOI: https://doi.org/10.1097/MOH.0000000000000202, PMID: 26554892

Drissen R, Buza-Vidas N, Woll P, Thongjuea S, Gambardella A, Giustacchini A, Mancini E, Zriwil A, Lutteropp M, Grover A, Mead A, Sitnicka E, Jacobsen SEW, Nerlov C. 2016. Distinct myeloid progenitor-differentiation pathways identified through single-cell RNA sequencing. *Nature Immunology* **17**:666–676. DOI: https://doi. org/10.1038/ni.3412, PMID: 27043410

Dykstra B, Kent D, Bowie M, McCaffrey L, Hamilton M, Lyons K, Lee SJ, Brinkman R, Eaves C. 2007. Long-term propagation of distinct hematopoietic differentiation programs in vivo. *Cell Stem Cell* **1**:218–229. DOI: https://doi.org/10.1016/j.stem.2007.05.015, PMID: 18371352

Dzierzak E, Philipsen S. 2013. Erythropoiesis: development and differentiation. *Cold Spring Harbor Perspectives in Medicine* **3**:a011601. DOI: https://doi.org/10.1101/cshperspect.a011601, PMID: 23545573

Galli SJ, Borregaard N, Wynn TA. 2011. Phenotypic and functional plasticity of cells of innate immunity: macrophages, mast cells and neutrophils. *Nature Immunology* **12**:1035–1044. DOI: https://doi.org/10.1038/ni.2109, PMID: 22012443

Gazit R, Mandal PK, Ebina W, Ben-Zvi A, Nombela-Arrieta C, Silberstein LE, Rossi DJ. 2014. Fgd5 identifies hematopoietic stem cells in the murine bone marrow. *The Journal of Experimental Medicine* **211**:1315–1331. DOI: https://doi.org/10.1084/jem.20130428, PMID: 24958848

Ginhoux F, Guilliams M. 2016. Tissue-resident macrophage ontogeny and homeostasis. *Immunity* **44**:439–449. DOI: https://doi.org/10.1016/j.immuni.2016.02.024, PMID: 26982352

Grzywacz B, Kataria N, Kataria N, Blazar BR, Miller JS, Verneris MR. 2011. Natural killer-cell differentiation by myeloid progenitors. *Blood* **117**:3548–3558. DOI: https://doi.org/10.1182/blood-2010-04-281394, PMID: 21173117

Harker LA, Roskos LK, Marzec UM, Carter RA, Cherry JK, Sundell B, Cheung EN, Terry D, Sheridan W. 2000. Effects of megakaryocyte growth and development factor on platelet production, platelet life span, and platelet function in healthy human volunteers. *Blood* **95**:2514–2522. PMID: 10753829

Havran WL, Allison JP. 1990. Origin of Thy-1+ dendritic epidermal cells of adult mice from fetal thymic precursors. *Nature* **344**:68–70. DOI: https://doi.org/10.1038/344068a0, PMID: 1968230

Hayakawa K, Hardy RR, Herzenberg LA, Herzenberg LA. 1985. Progenitors for Ly-1 B cells are distinct from progenitors for other B cells. *Journal of Experimental Medicine* **161**:1554–1568. DOI: https://doi.org/10.1084/jem.161.6.1554, PMID: 3874257

Kantor AB, Stall AM, Adams S, Watanabe K, Herzenberg LA. 1995. De novo development and self-replenishment of B cells. *International Immunology* **7**:55–68. DOI: https://doi.org/10.1093/intimm/7.1.55, PMID: 7536467

Kiel MJ, Yilmaz OH, Iwashita T, Yilmaz OH, Terhorst C, Morrison SJ. 2005. SLAM family receptors distinguish hematopoietic stem and progenitor cells and reveal endothelial niches for stem cells. *Cell* **121**:1109–1121. DOI: https://doi.org/10.1016/j.cell.2005.05.026, PMID: 15989959

Kiel MJ, Yilmaz OH, Morrison SJ. 2008. CD150- cells are transiently reconstituting multipotent progenitors with little or no stem cell activity. *Blood* **111**:4413–4414. DOI: https://doi.org/10.1182/blood-2007-12-129601, PMID: 18398056

Lu R, Neff NF, Quake SR, Weissman IL. 2011. Tracking single hematopoietic stem cells in vivo using high-throughput sequencing in conjunction with viral genetic barcoding. *Nature Biotechnology* **29**:928–933. DOI: https://doi.org/10.1038/nbt.1977, PMID: 21964413

Madisen L, Zwingman TA, Sunkin SM, Oh SW, Zariwala HA, Gu H, Ng LL, Palmiter RD, Hawrylycz MJ, Jones AR, Lein ES, Zeng H. 2010. A robust and high-throughput Cre reporting and characterization system for the whole mouse brain. *Nature Neuroscience* **13**:133–140. DOI: https://doi.org/10.1038/nn.2467, PMID: 20023653

Morrison SJ, Wandycz AM, Akashi K, Globerson A, Weissman IL. 1996. The aging of hematopoietic stem cells. *Nature Medicine* **2**:1011–1016. DOI: https://doi.org/10.1038/nm0996-1011, PMID: 8782459

Oguro H, Ding L, Morrison SJ. 2013. SLAM family markers resolve functionally distinct subpopulations of hematopoietic stem cells and multipotent progenitors. *Cell Stem Cell* **13**:102–116. DOI: https://doi.org/10.1016/j.stem.2013.05.014, PMID: 23827712

Palchaudhuri R, Saez B, Hoggatt J, Schajnovitz A, Sykes DB, Tate TA, Czechowicz A, Kfoury Y, Ruchika F, Rossi DJ, Verdine GL, Mansour MK, Scadden DT. 2016. Non-genotoxic conditioning for hematopoietic stem cell transplantation using a hematopoietic-cell-specific internalizing immunotoxin. *Nature Biotechnology* **34**:738–745. DOI: https://doi.org/10.1038/nbt.3584, PMID: 27272386

Paul F, Arkin Y, Giladi A, Jaitin DA, Kenigsberg E, Keren-Shaul H, Winter D, Lara-Astiaso D, Gury M, Weiner A, David E, Cohen N, Lauridsen FK, Haas S, Schlitzer A, Mildner A, Ginhoux F, Jung S, Trumpp A, Porse BT, et al. 2015. Transcriptional Heterogeneity and Lineage Commitment in Myeloid Progenitors. *Cell* **163**:1663–1677. DOI: https://doi.org/10.1016/j.cell.2015.11.013, PMID: 26627738

Pietras EM, Reynaud D, Kang YA, Carlin D, Calero-Nieto FJ, Leavitt AD, Stuart JM, Göttgens B, Passegué E. 2015. Functionally Distinct Subsets of Lineage-Biased Multipotent Progenitors Control Blood Production in Normal and Regenerative Conditions. *Cell Stem Cell* **17**:35–46. DOI: https://doi.org/10.1016/j.stem.2015.05.003, PMID: 26095048

Pronk CJ, Rossi DJ, Månsson R, Attema JL, Norddahl GL, Chan CK, Sigvardsson M, Weissman IL, Bryder D. 2007. Elucidation of the phenotypic, functional, and molecular topography of a myeloerythroid progenitor cell hierarchy. *Cell Stem Cell* **1**:428–442. DOI: https://doi.org/10.1016/j.stem.2007.07.005, PMID: 18371379

Rodvien R, Mielke CH. 1976. Role of platelets in hemostasis and thrombosis. *The Western Journal of Medicine* **125**:181–186. PMID: 969503

Rossi DJ, Bryder D, Zahn JM, Ahlenius H, Sonu R, Wagers AJ, Weissman IL. 2005. Cell intrinsic alterations underlie hematopoietic stem cell aging. *PNAS* **102**:9194–9199. DOI: https://doi.org/10.1073/pnas.0503280102, PMID: 15967997

Rundberg Nilsson A, Pronk CJ, Bryder D. 2015. Probing hematopoietic stem cell function using serial transplantation: Seeding characteristics and the impact of stem cell purification. *Experimental Hematology* **43**:812–817. DOI: https://doi.org/10.1016/j.exphem.2015.05.003, PMID: 26027791

Sanjuan-Pla A, Macaulay IC, Jensen CT, Woll PS, Luis TC, Mead A, Moore S, Carella C, Matsuoka S, Bouriez Jones T, Chowdhury O, Stenson L, Lutteropp M, Green JC, Facchini R, Boukarabila H, Grover A, Gambardella A, Thongjuea S, Carrelha J, et al. 2013. Platelet-biased stem cells reside at the apex of the haematopoietic stem-cell hierarchy. *Nature* **502**:232–236. DOI: https://doi.org/10.1038/nature12495, PMID: 23934107

Sawai CM, Babovic S, Upadhaya S, Knapp D, Lavin Y, Lau CM, Goloborodko A, Feng J, Fujisaki J, Ding L, Mirny LA, Merad M, Eaves CJ, Reizis B. 2016. Hematopoietic stem cells are the major source of multilineage hematopoiesis in adult animals. *Immunity* **45**:597–609. DOI: https://doi.org/10.1016/j.immuni.2016.08.007, PMID: 27590115

Säwén P, Lang S, Mandal P, Rossi DJ, Soneji S, Bryder D. 2016. Mitotic history reveals distinct stem cell populations and their contributions to hematopoiesis. *Cell Reports* **14**:2809–2818. DOI: https://doi.org/10.1016/j.celrep.2016.02.073, PMID: 26997272

Shin JY, Hu W, Naramura M, Park CY. 2014. High c-Kit expression identifies hematopoietic stem cells with impaired self-renewal and megakaryocytic bias. *The Journal of Experimental Medicine* **211**:217–231. DOI: https://doi.org/10.1084/jem.20131128, PMID: 24446491

Siminovitch L, McCulloch EA, Till JE. 1963. The distribution of colony-forming cells among spleen colonies. *Journal of Cellular and Comparative Physiology* **62**:327–336. DOI: https://doi.org/10.1002/jcp.1030620313, PMID: 14086156

Sudo K, Ema H, Morita Y, Nakauchi H. 2000. Age-associated characteristics of murine hematopoietic stem cells. *The Journal of Experimental Medicine* **192**:1273–1280. DOI: https://doi.org/10.1084/jem.192.9.1273, PMID: 11067876

Sun J, Ramos A, Chapman B, Johnnidis JB, Le L, Ho YJ, Klein A, Hofmann O, Camargo FD. 2014. Clonal dynamics of native haematopoiesis. *Nature* **514**:322–327. DOI: https://doi.org/10.1038/nature13824, PMID: 25296256

Till JE, McCulloch EA. 1961. A direct measurement of the radiation sensitivity of normal mouse bone marrow cells. *Radiation Research* **14**:213–222. DOI: https://doi.org/10.2307/3570892, PMID: 13776896

Ugale A, Norddahl GL, Wahlestedt M, Säwén P, Jaako P, Pronk CJ, Soneji S, Cammenga J, Bryder D. 2014. Hematopoietic stem cells are intrinsically protected against MLL-ENL-mediated transformation. *Cell Reports* **9**:1246–1255. DOI: https://doi.org/10.1016/j.celrep.2014.10.036, PMID: 25456127

Van Putten LM. 1958. The life span of red cells in the rat and the mouse as determined by labeling with DFP32 in vivo. *Blood* **13**:789–794. PMID: 13560578

Velten L, Haas SF, Raffel S, Blaszkiewicz S, Islam S, Hennig BP, Hirche C, Lutz C, Buss EC, Nowak D, Boch T, Hofmann WK, Ho AD, Huber W, Trumpp A, Essers MA, Steinmetz LM. 2017. Human haematopoietic stem cell lineage commitment is a continuous process. *Nature Cell Biology* **19**:271–281. DOI: https://doi.org/10.1038/ncb3493, PMID: 28319093

Weksberg DC, Chambers SM, Boles NC, Goodell MA. 2008. CD150- side population cells represent a functionally distinct population of long-term hematopoietic stem cells. *Blood* **111**:2444–2451. DOI: https://doi.org/10.1182/blood-2007-09-115006, PMID: 18055867

Westera L, Drylewicz J, den Braber I, Mugwagwa T, van der Maas I, Kwast L, Volman T, van de Weg-Schrijver EH, Bartha I, Spierenburg G, Gaiser K, Ackermans MT, Asquith B, de Boer RJ, Tesselaar K, Borghans JA. 2013. Closing the gap between T-cell life span estimates from stable isotope-labeling studies in mice and humans. *Blood* **122**:2205–2212. DOI: https://doi.org/10.1182/blood-2013-03-488411, PMID: 23945154

Wilson A, Laurenti E, Oser G, van der Wath RC, Blanco-Bose W, Jaworski M, Offner S, Dunant CF, Eshkind L, Bockamp E, Lió P, Macdonald HR, Trumpp A. 2008. Hematopoietic stem cells reversibly switch from dormancy to self-renewal during homeostasis and repair. *Cell* **135**:1118–1129. DOI: https://doi.org/10.1016/j.cell.2008.10.048, PMID: 19062086

Wu C, Li B, Lu R, Koelle SJ, Yang Y, Jares A, Krouse AE, Metzger M, Liang F, Loré K, Wu CO, Donahue RE, Chen ISY, Weissman I, Dunbar CE. 2014. Clonal tracking of rhesus macaque hematopoiesis highlights a distinct lineage origin for natural killer cells. *Cell Stem Cell* **14**:486–499. DOI: https://doi.org/10.1016/j.stem.2014.01.020, PMID: 24702997